ELSEVIER

Nuclear Physics A 617 (1997) 45–56

NUCLEAR PHYSICS A

Scattering of radioactive nuclei ^{6}He and ^{3}H by protons: Effects of neutron skin and halo in ^{6}He, ^{8}He, and ^{11}Li

A.A. Korsheninnikov[a,1], E.Yu. Nikolskii[b], C.A. Bertulani[c], S. Fukuda[a], T. Kobayashi[a], E.A. Kuzmin[b], S. Momota[a], B.G. Novatskii[b], A.A. Ogloblin[b], A. Ozawa[a], V. Pribora[b], I. Tanihata[a], K. Yoshida[a]

[a] *RIKEN, 2-1 Hirosawa, Wako, Saitama 351-01, Japan*

[b] *Kurchatov Institute, Kurchatov sq. 1, Moscow 123182, Russia*

[c] *Universidade Federal do Rio de Janeiro, 21945-970 Rio de Janeiro, Brazil*

Received 28 August 1996; revised 17 December 1996

Abstract

In an experimental study of ^{6}He+p and ^{3}H+p collisions at ~70 *A* MeV, the elastic scattering angular distributions were measured and the known excited state ^{6}He$^{*}_{1.8}$ was observed. Comparative analysis of existing experimental data on proton elastic scattering by ^{4}He, ^{6}He, ^{6}Li, ^{8}He, ^{9}Li, and ^{11}Li was performed. Effects of valence neutrons were investigated using the eikonal approach. A difference between ^{11}Li and ^{6,8}He was found. © 1997 Elsevier Science B.V.

PACS: 25.60.+v; 23.20.En; 21.10.Gv

Keywords: Nuclear reactions ^{1}H(^{6}He, p), (^{6}He, p^{4}He), (^{6}He, pn^{4}He), E = 71 MeV/nucleon; ^{1}H(^{3}H, p), E = 73.5 MeV/nucleon; Measured proton spectra; Sigma (theta); Analyzed sigma (theta) for beams ^{6}He, ^{8}He, ^{11}Li; Deduced neutron halo effects

1. Introduction

One of the most exciting events in nuclear physics of recent years was the discovery of extended neutron distributions in exotic neutron-rich nuclei like, e.g. ^{11}Li, ^{11}Be, ^{8}He, ^{6}He [1]. Such nuclei were experimentally studied mainly by cross sections measurements and fragmentation experiments [1,2]. Here we report on measurements of elastic scattering

[1] On leave from the Kurchatov Institute, Moscow 123182, Russia.

0375-9474/97/$17.00 © 1997 Elsevier Science B.V. All rights reserved.
PII S0375-9474(96)00492-7

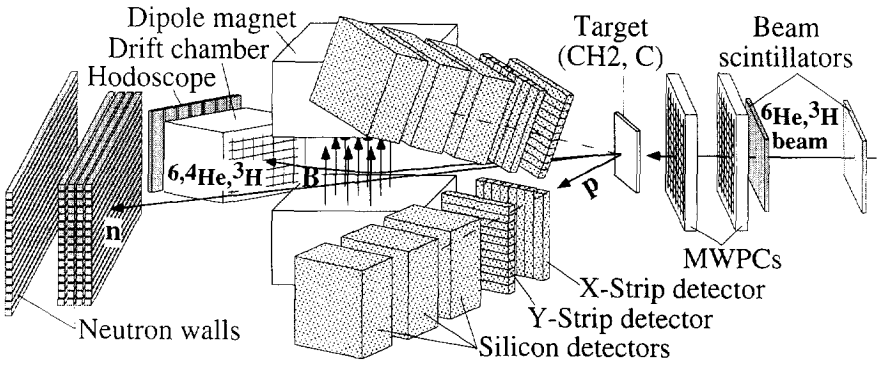

Fig. 1. The experimental setup.

of ^{6}He+p, which were performed together with a study of proton scattering by the radioactive nucleus ^{3}H. Another study of scattering of ^{6}He+p as well as ^{8}He+p was recently carried out in Ref. [3]; data analysis is in progress.

The extended neutron distributions sometimes are classified into two groups, neutron skins and neutron halos, reflecting the expectation of their different properties due to peculiar shapes of density profiles [1,4,5]. Below we perform a comparative analysis of all existing data on the proton elastic scattering by ^{6}He, ^{8}He, and ^{11}Li. It turns out that the proton does feel the valence neutrons in ^{6}He, ^{8}He and does not feel them in ^{11}Li, reflecting different properties of the neutron skin in ^{6}He, ^{8}He and the neutron halo in ^{11}Li.

2. Experimental method

The experiment was carried out in RIKEN (Japan). We used radioactive beams of ^{6}He and ^{3}H and studied ^{6}He+p and ^{3}H+p collisions under inverse kinematical conditions. We applied the missing mass method based on the detection of recoil protons both in an inclusive way and in coincidences with other emitted particles. The secondary beams were produced by the fragment separator RIPS from fragmentation of the ^{18}O primary beam at E = 100 A MeV on a ^{9}Be target with thickness 1.1 g/cm^2. The ^{6}He beam had an energy of E^{lab} = 71 A MeV with an energy spread $\Delta = \pm 3.0$ A MeV. The energy of the ^{3}H beam was E^{lab} = 73.5 A MeV ($\Delta = \pm 4.5$ A MeV).

The experimental setup is shown in Fig. 1. Two plastic scintillators and MWPCs were used for projectile identification, tracking, and measurement of the beam energy. The secondary beam hit CH_2 and C targets with thicknesses of 11.75 and 9.5 mg/cm^2, respectively. Note that all experimental distributions presented in this paper correspond to a pure proton target (negligible background from the C target was subtracted).

To detect protons, we used two telescopes of solid state detectors with large area. Every telescope consisted of two strip detectors and three silicon detectors. The centers of the telescopes were located at 69°, i.e. in the range of small center-of-mass angles

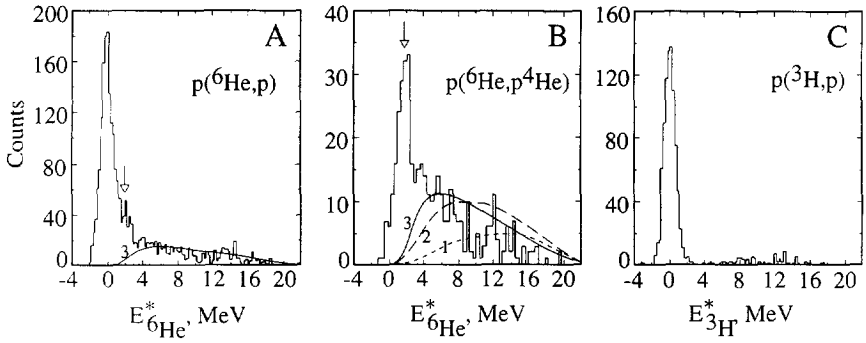

Fig. 2. Proton spectra from the processes indicated in the figure. Arrows show the position of the known excited state $^{6}He^{*}_{1.8}(2^{+})$. Curves show: (1) the phase space p+n+n+^{4}He; (2) the n+n final state interaction; (3) the n+^{4}He final state interaction via the resonance $^{5}He(3/2^{-})$.

in the scattering ^{6}He+p and ^{3}H+p. The telescopes measured energies and angles of every proton, which allowed us to determine the energy in the residual ^{6}He- or ^{3}H-like system. The resolution in the excitation energy of ^{6}He and ^{3}H (FWHM $\sim$ 1.5 MeV) was mainly due to the angular resolution of the setup and the target thickness.

In addition to the recoil protons, we detected other emitted particles. Charged particles were bent in the dipole magnet and measured by the drift chamber and the plastic scintillators' hodoscope. The hodoscope allowed us to determine the charge of the detected particle, while the drift chamber was used for isotope identification. Neutrons from the decay of ^{6}He were detected by layers of plastic scintillators. This part of the detection system allowed us to study exclusive spectra of protons detected in coincidences with particles from the projectile breakup.

3. Experimental results

To obtain the resulting spectra of protons presented in Fig. 2, we converted the measured distributions $d^2N/dE_p^{lab}d\Omega_p^{lab}$ into $d^2N/dE^*_{^{6}He(^{3}H)}d\Omega_p^{lab}$ and integrated them over angles within the acceptance of proton telescopes ($\theta_p^{lab} \sim 60$–$80°$). The inclusive spectrum of protons, in p(^{6}He, p), is presented in Fig. 2A. A strong peak corresponding to the ground state of ^{6}He is seen. The arrow corresponds to the known excited state of ^{6}He at $E^* = 1.8$ MeV ($J^{\pi} = 2^{+}$). This state is clearly seen in Fig. 2B, where we show the exclusive spectrum of protons detected in coincidences with ^{4}He. The observed width of the state is close to the experimental resolution, in agreement with the known narrow intrinsic width $\Gamma = 113$ keV. The proton spectrum detected in coincidences with ^{4}He and neutron also shows this state. In Figs. 2A and 2B, typical physical backgrounds are illustrated by curves which are smooth and follow the general trend in the high energy part of spectrum (detection acceptances and resolutions were taken into account in the calculations). Curve 1 corresponds to the phase space of p+n+n+^{4}He, curves

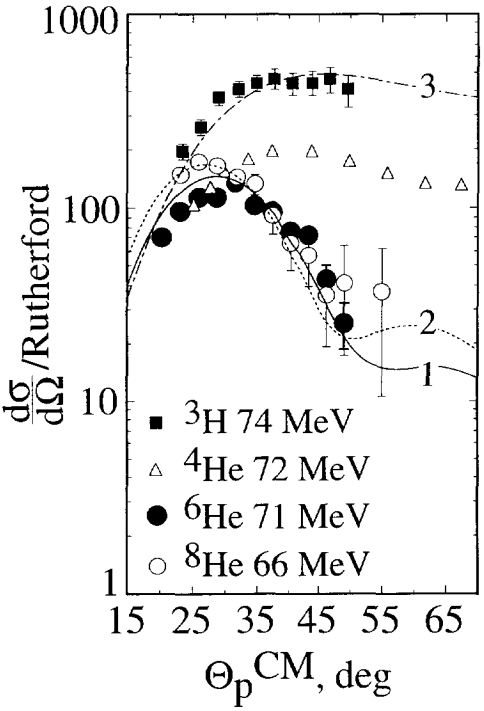

Fig. 3. Angular distributions as the ratio to the Rutherford cross section for the elastic of scattering ^{3}H+p at 74 A MeV, ^{6}He+p at 71 A MeV, ^{8}He+p at 66 A MeV [6], and p+^{4}He at 72 MeV [7]. Curves 1 and 2 show the optical model calculations for the scattering of ^{6}He+p and ^{8}He+p, respectively, using the same optical potential parameters found in Ref. [8] by a fit to the ^{8}He+p data from Ref. [9]. Curve 3 presents the optical model calculation for the scattering of ^{3}H+p using the potential parameters for the p+^{3}He scattering [10].

2 and 3 show calculations for the final state interactions of n+n (virtual state) and of n+^{4}He (the resonance ^{5}He($3/2^-$)), respectively. Fig. 2C shows the inclusive spectrum of protons from the process p(^{3}H, p). The elastic scattering peak is clearly seen.

The obtained angular distributions for the elastic scattering of ^{6}He+p and of ^{3}H+p are presented in Fig. 3 as a ratio to the Rutherford cross section. It is seen that the experimental points correspond predominantly to nuclear scattering (ratio to the Rutherford cross section is much larger than unity). In Fig. 3 we also show previously measured data for ^{8}He+p [6] and the data for ^{4}He+p [7] at center-of-mass energies close to that for the scattering of ^{6}He+p. It is seen that the results for ^{6}He+p and for ^{8}He+p are very similar to each other and differ essentially from the distribution for ^{4}He+p. To illustrate the resemblance of the results for ^{6}He and ^{8}He, we show in Fig. 3 the optical model calculations with identical potential parameters found in Ref. [8] for the elastic scattering of ^{8}He+p measured in Ref. [9] at a slightly higher energy of 73 A MeV. Curves 1 and 2 (for ^{6}He+p and ^{8}He+p, respectively) describe the experimental data well, reflecting a likeness of gross properties of ^{6}He and ^{8}He.

The cross sections $d\sigma/d\Omega_{\rm cm}$ for the elastic scattering of ^{6}He+p, ^{8}He+p and ^{4}He+p are shown in the middle of Fig. 4A. It is seen that the similarity between the results

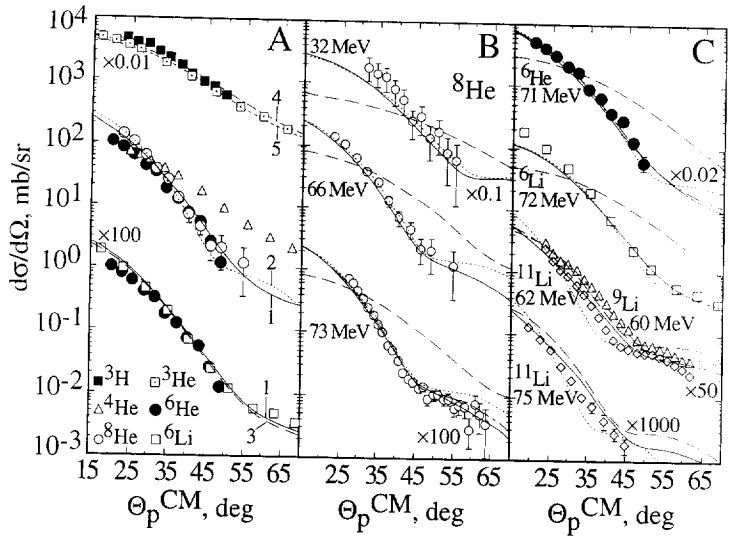

Fig. 4. (A) Cross sections for elastic scattering of p+^{3}H at 74 MeV, p+^{3}He at 85 MeV [10], p+^{4}He at 72 MeV [7], p+^{6}He at 71 MeV, p+^{8}He at 66 MeV [6], and p+^{6}Li at 72 MeV [11]. Curves present the optical model calculations: (1) for the scattering p+^{6}He using potential parameters for p+^{6}Li [11]; (2) for p+^{8}He using potential parameters found for scattering p+^{8}He at 72.5 MeV [8]; (3) for p+^{6}Li [11]; (4) for p+^{3}H using potential parameters for p+^{3}He [10]; (5) for p+^{3}He [10]. (B) Cross sections for elastic scattering of p+^{8}He at 32, 66, and 72.5 MeV [12,6,9]. Curves show the eikonal calculations (see the text). (C) Cross sections for elastic scattering of p+^{6}He at 71 MeV, p+^{6}Li at 72 MeV [11], p+^{11}Li at 62 MeV [13], p+^{9}Li at 60 MeV [13], and p+^{11}Li at 75 MeV [6]. Curves show the eikonal calculations (see the text).

for ^{6}He, ^{8}He and their difference from ^{4}He+p scattering are manifested via the slopes of angular distributions. In the case of predominance of nuclear scattering (see Fig. 3), the slopes of the angular distributions usually are determined mainly by the matter radii. Thus the observed specific features of the experimental data show, on the one hand, that the radii of ^{6}He and ^{8}He are close to each other and, on the other hand, that the radii of ^{6}He and ^{8}He are larger than that of an α-particle. This is in agreement with the experimental values of the radii, $R_{mat}(^6\text{He}) = 2.48 \pm 0.03$ fm or 2.57 ± 0.1 fm [14,15], $R_{mat}(^8\text{He}) = 2.52 \pm 0.03$ fm [14], $R_{mat}(^4\text{He}) \approx 1.48$ fm [16].

In Fig. 4A, curve 1 presents the calculation for the elastic scattering of ^{6}He+p with the optical potential obtained in Ref. [11] for the elastic scattering of p+^{6}Li at almost the same energy of 72 MeV (note that we studied the ^{6}He+p scattering at 71 A MeV). This curve agrees well with the experimental data. The experimental data for ^{6}He+p and ^{6}Li+p measured at almost the same energy are compared in the bottom of Fig. 4A. It is seen that these angular distributions are almost identical. This fact reveals a close similarity between gross characteristics of density distributions in ^{6}He and ^{6}Li. Note that the radii of ^{6}He and ^{6}Li are really close to each other, $R_{mat}(^6\text{Li}) = 2.44 \pm 0.1$ fm [16] and $R_{mat}(^6\text{He}) = 2.48 \pm 0.03$ fm or 2.57 ± 0.1 fm [14,15], while a close analogy between the geometrical structures of ^{6}He and ^{6}Li is seen in three-body calculations [17,18] (in spite of different spin-parities and other particularities of these ground states).

The measured cross section for the elastic scattering of ^{3}H+p at 74 A MeV is compared with data for elastic scattering of p+^{3}He at 85 MeV [10] on the top of Fig. 4A. Curve 4 shows the optical model calculation for ^{3}H+p using the potential parameters found in Ref. [10] for the p+^{3}He data; the latter calculation for p+^{3}He is presented by curve 5 in Fig. 4A (the calculation for ^{3}H+p is also shown by curve 3 in Fig. 3). Again, the results for the scattering of ^{3}H+p and ^{3}He+p are in close agreement in consistency with ^{3}H and ^{3}He belonging to the same isospin doublet.

4. Effects of extended neutron distributions in ^{6}He, ^{8}He and ^{11}Li

The performed measurement of elastic scattering of ^{6}He+p has enlarged the bank of experimental data on proton scattering by nuclei with neutron skin or halo. Fig. 4B and 4C show all existing data for the elastic scattering ^{8}He+p at 73, 66, and 32 A MeV, ^{6}He+p at 71 A MeV, ^{11}Li+p at 62 and 75 A MeV (present experiment and Refs. [6,9,12,13]). In Fig. 4C we also show data for the elastic scattering of p+^{6}Li at 72 MeV [11]. The ^{6}Li nucleus was included in our analysis because it can be considered as an α-core and an extended neutron+proton distribution. Below we analyze the data presented in Figs. 4B and 4C using the eikonal approach, which attracts attention because it has no fitting parameters and provides a straightforward connection with the densities of nuclei. A satisfactory application of the eikonal approach in the energy range under consideration was established in several papers. For example, in Ref. [19] it was found that this approximation works well up to the second maximum in the angular distributions for light nuclei. Note also that the energies under consideration correspond to the limit of applicability of the eikonal approximation, and development of a precise theory for elastic scattering in this energy domain is strongly needed.

We used the following amplitude for proton–nucleus elastic scattering [20]:

$$f = ik \int_0^\infty J_0 \left(e^{i\chi_C} - e^{i\chi_C + i\chi_N} \right) b\, db + f_C ,$$

$$\chi_N(b) = -\frac{1}{\hbar v} \int_{-\infty}^{\infty} dz\, V_N \left(\sqrt{b^2 + z^2} \right) , \qquad (1)$$

where $k^2 = 2\mu E_{CM}/\hbar^2$, f_C is the standard Coulomb amplitude [20] and χ_C is the Coulomb phase for a uniform charged sphere with $R_c = r_{oc}A^{1/3}$ (r_{oc} = 1.33 fm for ^{9}Li and 1.1 fm for ^{4}He [21]). The nuclear phase χ_N is determined by the optical potential $V_N = \langle t_{pn} \rangle \rho_n + \langle t_{pp} \rangle \rho_p$ with $\langle t_{pN} \rangle = -\hbar v \bar{\sigma}_{pN}(a_{pN} + i)/2$ [20]. Here ρ_p and ρ_n are proton and neutron densities of nucleus, respectively. They will be discussed below. The Pauli-corrected proton–nucleon total cross section, $\bar{\sigma}_{pN} = \sigma_{pN} P(\epsilon_{NF}/\epsilon)$, was derived in Ref. [22]. The correction term P depends on the Fermi energy, ϵ_{NF}, of the struck target nucleon, which was calculated for the proton and neutron densities, $\rho_{p(n)}$; to evaluate the energy ϵ of the incident proton at the interaction point we used the Coulomb potential

and the real part of potential V_N (an analogous procedure was used in Ref. [23]; see also Ref. [22]).

In addition to the densities $\rho_{n(p)}$, the input for the calculations includes parameters of the pN amplitude, σ_{pN} and α_{pN}. The pp and pn total cross sections, σ_{pN}, are known at energies under consideration, $E \leqslant 100$ MeV (see, e.g. Ref. [24]); we approximated them by $\sigma_{pp}[\text{mb}] = 1/(-1.4 \times 10^{-3} + 4.45 \times 10^{-4}E - 7.37 \times 10^{-7}E^2)$ and $\sigma_{pn}[\text{mb}] = 1/(-2.5 \times 10^{-4} + 1.15 \times 10^{-4}E + 1.73 \times 10^{-7}E^2)$ (E in MeV). The parameters α_{pN} are known at $E \geqslant 100$ MeV [25]. We used interpolations, $\alpha_{pp} = 2.55 - 6.8 \times 10^{-3}E$ and $\alpha_{pn} = 1.08\text{–}8.0 \times 10^{-4}E$, from the values of α_{pN} [25] at the two lowest energies.

To investigate the sensitivity of the elastic scattering to the neutron skin or halo, we performed calculations for every nucleus considering three kinds of densities $\rho_{n(p)}$:

(i) The "*realistic*" densities, which contain the extended distribution of valence nucleons and correspond to the experimental matter radius of ^{8}He, ^{6}He, ^{6}Li, or ^{11}Li.

These densities were derived in the cluster-orbital shell-model approximation (COSMA) [26] based on the approach from Ref. [27]. For ^{11}Li, we used the following neutron and proton densities from Ref. [26] obtained in the ^{9}Li+2n model:

$$\rho_i(r) = N_{ci}\frac{\exp(-r^2/a^2)}{\pi^{3/2}a^3} + N_{vi}\frac{2\exp(-r^2/b^2)}{3\pi^{3/2}b^5}\left[Ar^2 + B\left(r^2 - \frac{3}{2}b^2\right)^2\right], \qquad (2)$$

$$i = \text{n, p},$$

where $N_{cp} = 3$, $N_{cn} = 6$, $N_{vp} = 0$, $N_{vn} = 2$, $a = 1.89$ fm, $b = 3.68$ fm, $A = 0.81$, $B = 0.19$. These densities contain the neutron halo, yielding $R_{mat}(^{11}\text{Li}) = 3.2$ fm in agreement with the experimental value [1,14], and corresponding to a mixture of 1p and 2s orbitals for the valence neutrons. This mixture allows one to reproduce experimental data on transverse momentum distributions of ^{9}Li from fragmentation of ^{11}Li [26]. Different orbitals for the valence neutrons were investigated in Ref. [6] and were found to give results close to the solid curves for ^{11}Li in Fig. 4C, which represent calculations using Eq. (3).

The densities of ^{8}He were derived in the α+4n model of Ref. [28] and can be written as Eq. (3) with $N_{vn} = 4$, $N_{vp} = 0$, $N_{cp} = N_{cn} = 2$, $a = 1.38$ fm, $b = 1.99$ fm, $A = 1$, $B = 0$. These densities reproduce the experimental radius of ^{8}He, $R_{mat}(^8\text{He}) = 2.52$ fm [14], and contain an extended neutron distribution. In this case in Eq. (3) a Gaussian density of ^{4}He was used which was then folded with a Gaussian form for motion of the ^{4}He core in ^{8}He. We also tried a more sophisticated wave function of ^{4}He, which was obtained in the resonating group method [29]. The result shown in Fig. 4B, with an example of the scattering of ^{8}He+p at 73 A MeV by dot–dashed curve, is close to the solid curve calculated using Eq. (3).

The densities of ^{6}He and ^{6}Li, which we obtained in the $\alpha + 2$N model, can be written in the form of Eq. (3) with $A = 1$, $B = 0$, $N_{cp} = N_{cn} = 2$; $N_{vn} = N_{vp} = 1$ for ^{6}Li and $N_{vn} = 2$, $N_{vp} = 0$ for ^{6}He; $a = 1.55$ fm corresponds to a Gaussian density for ^{4}He($R_{mat}(^4\text{He}) = 1.48$ fm) folded with a Gaussian form of motion of the ^{4}He-core in ^{6}He or ^{6}Li, which is characterized by $R_{rms} = 1.2$ fm for both ^{6}He and ^{6}Li [18,26].

The parameter b was chosen to reproduce the experimental radius of ^{6}He and ^{6}Li: b = 2.07 fm for $R_{mat}(^6Li)$ = 2.45 fm and b = 2.24 fm for $R_{mat}(^6He)$ = 2.57 fm [15]. (The calculation with b = 2.12 fm for $R_{mat}(^6He)$ = 2.48 fm [14], which is shown in Fig. 4C by the dot–dashed curve, is very close to the solid curve for $R_{mat}(^6He)$ = 2.57 fm.)

(ii) The second group of calculations was performed using the "*non-halo*" densities which neglect the difference between the proton and neutron radii, but correspond to the experimental matter radius of ^{8}He, ^{6}He, ^{6}Li, or ^{11}Li. We used the Gaussian proton and neutron densities with identical radii equal to $R_{mat}(^8He)$ = 2.52 fm, $R_{mat}(^6He)$ = 2.57 fm, $R_{mat}(^6Li)$ = 2.45 fm or $R_{mat}(^{11}Li)$ = 3.2 fm.

(iii) The third group of calculations corresponds to the "*core-like*" densities. In this case we neglected the neutron skin or halo and replaced the real matter radius of the nucleus by the radius of the core (^{4}He or ^{9}Li). Namely, we used the Gaussian proton and neutron densities with identical radii equal to $R_{mat}(^4He)$ = 1.48 fm for ^{8}He, ^{6}He, ^{6}Li and $R_{mat}(^9Li)$ = 2.32 fm [14] for ^{11}Li.

Results of calculations with the "*realistic*" densities, which correspond to the experimental matter radius of ^{8}He, ^{6}He, ^{6}Li, or ^{11}Li and contain the extended distribution of valence nucleons, are shown in Figs. 4B and 4C by solid curves. They are in reasonable agreement with all experimental data. Calculations with the "*non-halo*" densities, which correspond to the experimental matter radius of ^{8}He, ^{6}He, ^{6}Li or ^{11}Li, but neglect a difference between proton and neutron radii, are shown by dotted curves in Figs. 4B and 4C. It is seen that for ^{8}He, ^{6}He, ^{6}Li (but not for ^{11}Li) these curves are close to the solid curves being in reasonable agreement with the experimental points. At the same time the dashed curves, which correspond to the "*core-like*" densities (the neutron skin or halo is neglected, and the real matter radius of the nucleus is replaced by the radius of the core), differ drastically from the experimental data, solid and dotted curves for ^{8}He, ^{6}He and ^{6}Li. These results indicate that the proton elastic scattering is sensitive to the matter extension in ^{8}He, ^{6}He and ^{6}Li in comparison with the α-particle and it is insensitive to the difference between proton and neutron radii in ^{8}He and ^{6}He.

Such observations are different for the scattering of ^{11}Li+p. As seen in Fig. 4C, the solid curves are more similar to the dashed curves than to the dotted ones. A big similarity between the solid curve ("*realistic*" density) and the dashed curve ("*core-like*" density) show that the ^{11}Li+p scattering is determined to a large extent by the proton scattering on the ^{9}Li core, reflecting a low-density in the neutron halo. Since the density of valence neutrons is lower in the ^{11}Li halo than in ^{6,8}He, the transparency of the halo for the incoming proton is larger in ^{11}Li than in ^{6,8}He. As a result, the proton penetrates through the halo in ^{11}Li and scatters on the ^{9}Li core unlike the case of ^{6,8}He. Note, that essentially different transparencies of the ^{11}Li halo and of the ^{6}He neutron skin can be understood from a simple consideration of the mean free path of the proton in the matter of the halo/skin. The mean free path depends on the proton–neutron cross section, which is the same for cases of ^{11}Li and ^{6}He (proton energies are close to each other), and on the density, that is on the volume of halo/skin, where the two valence neutrons are distributed. If the halo in ^{11}Li and the skin in ^{6}He would have the same thickness (actually the ^{11}Li halo is even thicker), the volume of the ^{11}Li halo would be

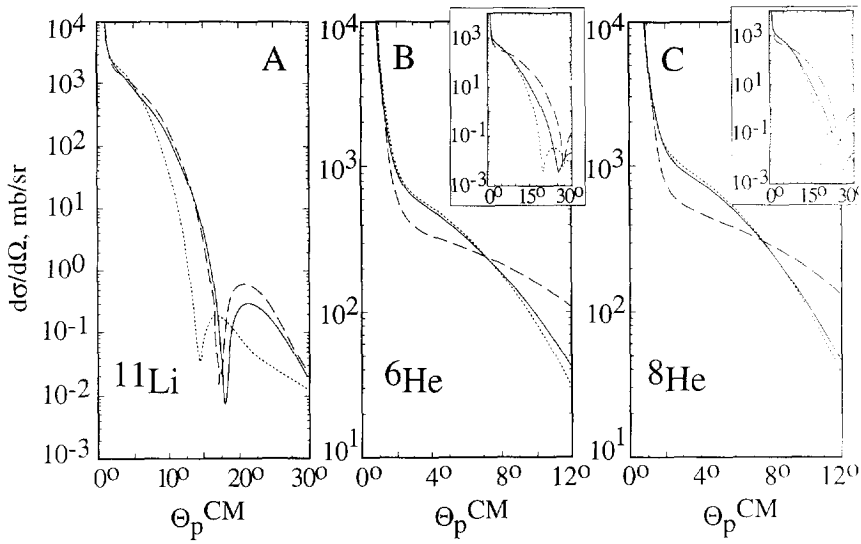

Fig. 5. Eikonal calculations (see the text) of cross sections for elastic scattering of (A) ^{11}Li+p, (B) ^{6}He+p, and (C) ^{8}He+p all three at 800 A MeV. Inserts in (B) and (C) show the angular distributions in a wider angular range corresponding to the four momentum transfer squared, $|t| \leqslant 0.5$ (GeV/c)^2.

already essentially larger than that in ^{6}He, just because in ^{11}Li the halo is located on the top of the core with a larger radius ($R_{^9\mathrm{Li}} > R_\alpha$). Finally, the mean free path, which strongly depends on the density (the density appears in an exponent), is essentially larger for ^{11}Li than for ^{6}He.

The difference between ^{11}Li and ^{6,8}He is also seen directly from the experimental data. In Fig. 4C, the ^{11}Li data at 62 A MeV is compared with the data for ^{9}Li+p scattering [13] shown by triangles (the dashed-dotted curve shows the eikonal calculation for ^{9}Li+p and describes the data well). These ^{11}Li and ^{9}Li distributions have very similar slopes and shapes unlike the case of He isotopes in the middle of Fig. 4A, where the slope of the angular distribution for ^{4}He differs essentially from that for ^{6,8}He. Note that the similarity of the angular distributions for ^{11}Li+p and ^{9}Li+p was also discussed in Refs. [30,31], where the fragile ^{11}Li halo was found to be responsible for additional absorption and a lower cross section in comparison with that for ^{9}Li. If a proton hits the ^{9}Li core after penetrating through the halo, it is easy to shake off the valence neutrons, which are loosely bound.

Such a distinction of ^{11}Li from ^{8}He, ^{6}He, ^{6}Li remains at high energy proton scattering. Fig. 5A shows calculations for the elastic scattering of ^{11}Li+p at 800 A MeV (the Np amplitude parameters were taken from [25]). It is seen that the solid curve for the "*realistic*" density is close in a wide angular range to the dashed curve for the "*core-like*" density (the result that ^{11}Li and ^{9}Li theoretically give rise to a very similar angular distributions was also obtained in Ref. [32]). At the same time, both curves differ from

the dotted curve ("*non-halo*" densities). Considering the 800 MeV proton scattering by ^{6}He and ^{8}He in Fig. 5B and 5C at angles $\leqslant 10°$, that is at low values of the four momentum transfer squared, $|t| \leqslant 0.05$ (GeV/c)^2, we see that the situation differs from the ^{11}Li case. Unlike Fig. 5A, in Figs. 5B and 5C the solid curves are close to the dotted curves and differ from the dashed curves. At larger angles all three curves have distinctive behaviors (see inserts in Figs. 5B and 5C) showing that the high energy proton scattering, being studied at relatively large angles corresponding to $|t| \sim 0.1$–0.5 (GeV/c)^2, may allow one to extract detailed information about the ^{8}He and ^{6}He density distributions. Note that detailed theoretical studies of elastic scattering ^{8}He+p were performed in Refs. [33,34].

Thus, the present study has revealed that (i) the proton scattering by ^{8}He, ^{6}He, ^{6}Li at low energies (and at small angles at high energies) is not sensitive to a difference in neutron and proton distributions, but it is sensitive to the matter radius of ^{8}He, ^{6}He, ^{6}Li, i.e. feels the density extension in these nuclei in comparison with the α-particle; (ii) on the contrary, the elastic scattering ^{11}Li+p is mainly determined by the proton scattering on the ^{9}Li core being not sensitive to the neutron halo extended beyond the ^{9}Li core. These results demonstrate a difference between the properties of the extended neutron distributions in ^{11}Li, on the one hand, and ^{8}He or ^{6}He, on the other hand, and form a basis for distinction between the neutron skin in ^{8}He, ^{6}He and the halo in ^{11}Li.

5. Summary

We have performed an experimental study of collisions of ^{6}He+p and ^{3}H+p at 71 and 73.5 A MeV, respectively, applying the missing mass method based on a detection of recoil protons both in an inclusive way and in coincidence with other emitted particles. Angular distributions for the elastic scattering of ^{6}He+p and ^{3}H+p were measured and the known excited state of ^{6}He at $E^* = 1.8$ MeV was observed.

Comparison of the measured angular distributions with other experimental data on proton scattering by ^{8}He, ^{4}He, ^{3}He has demonstrated that (i) results for ^{6}He and ^{8}He are very similar to each other and differ essentially from that for ^{4}He reflecting that ^{6}He and ^{8}He have matter radii greater than that of the α-particle in agreement with the experimental values of these radii; (ii) angular distributions for the proton scattering by ^{6}He and ^{6}Li are almost identical showing resemblance between gross characteristics of density distributions in ^{6}He and ^{6}Li; (iii) results for ^{3}H and ^{3}He are in an intimate agreement in consistency with a belonging of these nuclei to the same isospin doublet.

Effects of the valence nucleons in the proton scattering by ^{6}He, ^{6}Li, ^{8}He, and ^{11}Li were analyzed using the eikonal approach and it was revealed that (i) the scattering of ^{8}He, ^{6}He, ^{6}Li at low energies (and at small angles at high energies) is not sensitive to a difference in neutron and proton distributions, but it is sensitive to the matter radius of these nuclei, i.e. feels the density extension in these nuclei in comparison with the α-particle; (ii) on the contrary, the elastic scattering ^{11}Li+p is mainly determined by the proton scattering on the ^{9}Li core being not much sensitive to the low-density neutron

halo extended beyond the ^{9}Li core. This different sensitivity to the valence neutrons in ^{6,8}He and ^{11}Li is confirmed by a direct comparison of the experimental data for ^{6,8}He+p and ^{4}He+p, on the one hand, and for ^{11}Li+p and ^{9}Li+p, on the other hand. These results form a basis for distinction between the neutron skin in ^{8}He, ^{6}He and the neutron halo in ^{11}Li. At the same time, as was shown in Ref. [6], the proton elastic scattering is not a very promising tool to study the fine details of halos like, e.g. orbitals of valence neutrons in ^{11}Li.

Acknowledgements

This work was supported in part by Grant-in-Aid for Scientific Research on Priority Areas (No 05243102) from the Ministry of Education, Science and Culture.

References

[1] I. Tanihata, Prog. Part. Nucl. Phys. 35 (1995) 505.
[2] H. Geissel, G. Munzenberg and K. Riisager, Ann. Rev. Nucl. Part. Sci. 45 (1995) 163.
[3] S. Neumaier, G.D. Alkhazov, M.N. Andronenko, T. Beha, K.-H. Behr, A. Brunle, K. Burkhard, A.V. Dobrovolsky, P. Egelhof, C. Fischer, G.E. Gavrilov, H. Geissel, V.I. Iatsoura, H. Irnich, A.V. Khanzadeev, G.A. Korolev, A.A. Lobodenko, P. Lorenzen, G. Munzenberg, M. Mutterer, F. Nickel, W. Schwab, D.M. Seliverstov, P. Singer, T. Suzuki, J.P. Theobald, N.A. Timofeev and A.A. Vorobyov, Nucl. Phys. A 583 (1995) 799c.
[4] N. Fukunishi, T. Otsuka and I. Tanihata, Phys. Rev. C 48 (1993) 1648.
[5] K. Riisager, Rev. Mod. Phys. 66 (1994) 1105.
[6] A.A. Korsheninnikov, E.Yu. Nikolskii, T. Kobayashi, A. Ozawa, S. Fukuda, E.A. Kuzmin, S. Momota, B.G. Novatskii, A.A. Ogloblin, V. Pribora, I. Tanihata and K. Yoshida, Phys. Rev. C 53 (1996) R537.
[7] S. Burzynski, J. Campbell, M. Hammans, R. Henneck, W. Lorenzon, M.A. Pickar and I. Sick, Phys. Rev. C 39 (1989) 56.
[8] S.A. Goncharov and A.A. Korsheninnikov, Europhys. Lett. 30 (1995) 13.
[9] A.A. Korsheninnikov, K. Yoshida, D.V. Aleksandrov, N. Aoi, Y. Doki, N. Inabe, M. Fujimaki, T. Kobayashi, H. Kumagai, C.-B. Moon, E.Yu. Nikolskii, M.M. Obuti, A.A. Ogloblin, A. Ozawa, S. Shimoura, T. Suzuki, I. Tanihata, Y. Watanabe and M. Yanokura, Phys. Lett. B 316 (1993) 38.
[10] L.G. Votta, P.G. Roos, N.S. Chant and R. Woody, III, Phys. Rev. C 10 (1974) 520.
[11] R. Henneck, G. Masson, P.D. Eversheim, R. Gebel, F. Hinterberger, U. Lahr, H.W. Schmitt, J. Schleef and B.V. Przewoski, Nucl. Phys. A 571 (1994) 541.
[12] A.A. Korsheninnikov, E.Yu. Nikolskii, T. Kobayashi, D.V. Aleksandrov, M. Fujimaki, H. Kumagai, A.A. Ogloblin, A. Ozawa, I. Tanihata, Y. Watanabe and K. Yoshida, Phys. Lett. B 343 (1995) 53.
[13] C.-B. Moon, M. Fujimaki, S. Hirenzaki, N. Inabe, K. Katori, J.C. Kim, Y.K. Kim, T. Kobayashi, T. Kubo, H. Kumagai, S. Shimoura, T. Suzuki and I. Tanihata, Phys. Lett. B 297 (1992) 39.
[14] I. Tanihata, T. Kobayashi, O. Yamakawa, S. Shimoura, K. Ekuni, K. Sugimoto, N. Takahashi, T. Shimoda and H. Sato, Phys. Lett. B 206 (1988) 592.
[15] L.V. Chulkov, B.V. Danilin, V.D. Efros, A.A. Korsheninnikov and M.V. Zhukov, Europhys. Lett. 8 (1989) 245.
[16] R.G. Barret and D.F. Jackson, Nuclear Sizes and Structure (Clarendon, Oxford, 1977).
[17] V.I. Kukulin, V.M. Krasnopol'sky, V.T. Voronchev and P.B. Sazonov, Nucl. Phys. A 453 (1986) 365.
[18] B.V. Danilin, M.V. Zhukov, A.A. Korsheninnikov and L.V. Chulkov, Sov. J. Nucl. Phys. 53 (1991) 45 [Yad. Fiz. 53 (1991) 71].
[19] I. Brissaud, L. Bimbot, Y.Le. Bornec, B. Tatischeff and N. Willis, Phys. Rev. C 11 (1975) 1537.
[20] C.A. Bertulani, L.F. Canto and M.S. Hussein, Phys. Rep. 226 (1993) 281.
[21] C.M. Perey and F.G. Perey, Nucl. Data Tables 10 (1972) 539.

[22] E. Clementel and C. Villi, Nuovo Cimento II (1955) 176.
[23] G.W. Greenless, G.J. Pyle and Y.C. Tang, Phys. Rev. 171 (1968) 1115.
[24] W.O. Lock and D.F. Measday, Intermediate Energy Nuclear Physics (Menthuen, London, 1970).
[25] L. Ray, Phys. Rev. C 20 (1979) 1857.
[26] M.V. Zhukov, B.V. Danilin, D.V. Fedorov, J.M. Bang, I.S. Thompson and J.S. Vaagen, Phys. Rep. 231 (1993) 151.
[27] Y. Suzuki and K. Ikeda, Phys. Rev. C 38 (1988) 410.
[28] M.V. Zhukov, A.A. Korsheninnikov and M.H. Smedberg, Phys. Rev. C 50 (1994) R1.
[29] D.R. Thompson, R.E. Brown, M. LeMere and Y.C. Tang, Phys. Rev. C 16 (1977) 1.
[30] S. Hirenzaki, H. Toki and I. Tanihata, Nucl. Phys. A 552 (1993) 57.
[31] Y. Suzuki, K. Yabana and Y. Ogawa, Phys. Rev. C 47 (1993) 1317.
[32] G.D. Alkhazov and A.A. Lobodenko, Phys. At. Nuclei 56 (1993) 337.
[33] L.V. Chulkov, C.A. Bertulani and A.A. Korsheninnikov, Nucl. Phys. A 587 (1995) 291.
[34] R. Crespo, J.A. Tostevin and R.C. Johnson, Phys. Rev. C 51 (1995) 3283.